JOURNAL OF AIRCRAFT
Vol. 38, No. 6, November–December 2001

Methodology for Supersonic Panel Flutter Analysis of Thermal Protection System Seals

Guangfeng Cheng* and Chuh Mei†
Old Dominion University, Norfolk, Virginia 23529-0247
and
Roger R. Chen‡
Lockheed Martin Engineering and Science Corporation, Hampton, Virginia 23681-0001

A methodology is presented for the flutter analysis of the seal of the thermal protection system panel of the X-33 Advanced Technology Demonstrator test vehicle. The seal is simulated as a two-dimensional cantilevered panel with an elastic stopper, which is modeled as an equivalent spring. This cantilever beam–spring model under the aerodynamic pressure at supersonic speeds becomes an impact nonlinear dynamic system. The flutter analysis of the seal is, thus, carried out using time-domain numerical simulation with a displacement stability criterion. The flutter boundary of the seal is further verified with a family of three traditional and one nontraditional panel flutter models. The frequency-domain method that applies eigenanalysis on the traditional panel flutter problem was used. The results showed that the critical dynamic pressure could be more than doubled with the properly chosen material for the base stopper. The proposed methodology can be easily extended to three-dimensional panel seals with flow angularity.

Nomenclature

$[a_a]$, $[A_a]$	=	element and system aerodynamic influence matrices
b	=	beam width
C_a	=	aerodynamic damping coefficient
$\{d\}$	=	element nodal displacement vector
E	=	Young's modulus
F_e	=	impact force
$[g]$, $[G]$	=	element and system aerodynamic damping matrices
g_a	=	nondimensional aerodynamic damping
h	=	beam thickness
I	=	area moment of inertia
$[K_e]$, $[K]$	=	element and system stiffness matrices
k_s	=	equivalent spring stiffness
L	=	beam length
M_∞	=	Mach number
$[m]$, $[M]$	=	element and system mass matrices
$\lfloor N \rfloor$	=	beam element shape functions
P_a	=	aerodynamic pressure
$\{Q_e\}$, $\{Q\}$	=	element and system load vectors
q	=	dynamic pressure
V	=	airflow speed
$\{W\}$	=	system nodal displacement vector
W_e	=	transverse deflection at beam free end
w	=	transverse displacement
α	=	panel damping rate
κ	=	nondimensional eigenvalue
λ	=	nondimensional dynamic pressure
μ	=	mass ratio
ρ, ρ_a	=	beam and air mass densities
$\{\Phi\}$	=	eigenvector
Ω	=	complex panel motion parameter
ω, ω_0	=	panel and reference frequencies

Received 1 November 1999; revision received 30 November 2000; accepted for publication 28 December 2000.

*Graduate Student, Aerospace Engineering Department.
†Professor, Aerospace Engineering Department. Associate Fellow AIAA.
‡Aerospace Engineer, Space Operations Department.

Introduction

VARIOUS methods have been employed to solve the panel flutter[1,2] problem, which is among the general considerations for designing structures under supersonic/hypersonic conditions. In dynamics, the flutter boundary generally takes the form of critical nondimensional dynamic pressure. The solution means can be classified into two categories[3]: frequency-domain methods and time-domain methods. While using finite element analysis, frequency-domain methods are feasible when the problem can be cast as an eigenvalue problem. However, when it is mathematically difficult to execute eigenanalysis, time-domain methods can be applied for determining flutter. The acceptability of the results depends on the numerical stability of the methods adopted.

The problem cited in this paper arises from the stability analysis of the seal of a superalloy honeycomb thermal protection system (TPS) panel of the X-33 vehicle.[4] Figure 1 is from the blueprint of the seal for two adjacent TPS panels. The vibration of the covering seal is restrained with the neighboring panel. As the overhead airflow speed increases, flutter will occur. The seal is restrained to move downward by the top surface of the adjacent panel, and a tiny gap (or zero gap) exists between the seal and the adjacent panel. Therefore, a simplified two-dimensional model for the seal (flow angle $\Lambda = 0$ deg) is idealized as a cantilever beam with a stopper below its free end, as shown in Fig. 2. Accordingly, the problem becomes a vibration problem with an impact at some amplitude.

If the stopper is very stiff, so that it can be taken as a rigid stopper, the beam will undergo impact force during its vibration, and a restitution coefficient can be included to allow for energy loss.[5] However, the stopper should be treated as elastic; thus, more factors require consideration. For this case, an equivalent spring can be used to replace the stopper. In an investigation of the family of beams with the left end clamped and the right end using various supports as shown in Fig. 3, flutter analysis of the spring stopper model as well as the bar stopper model, which is closer to real flutter problem, belongs to nontraditional panel flutter analysis. In the present paper, the time-domain method is developed and employed to solve this nontraditional flutter problem. Apparently, the flutter of models I, IV, and V in Fig. 3 comprises traditional panel flutter analysis because eigenanalysis is applicable.

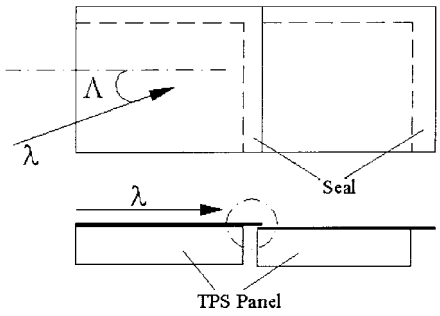

Fig. 1 TPS panel configuration.

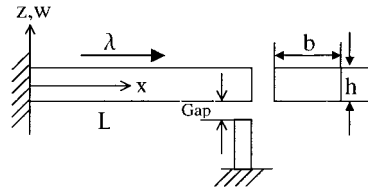

Fig. 2 Cantilever beam with stopper.

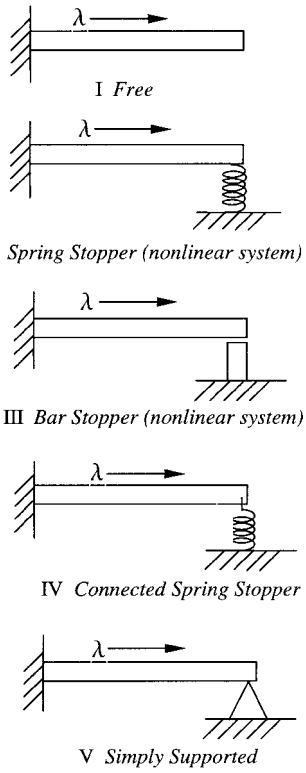

Fig. 3 Various support conditions at the right end.

The systematic procedures of finite element analysis were followed, with consideration given to the aerodynamic effect with quasi-steady first-order piston theory. For the spring stopper model, the equivalent spring stiffness is from the assumption that the stopper undergoes elastic deformation. Thus, the impact force is the restitution force of the equivalent spring. The main interest was focused on the variation of critical dynamic pressure vs stopper stiffness. The flutter boundary was compared with those of similar cases with simpler boundary conditions.

Finite Element Formulation

The classical Euler–Bernoulli beam element can be extended with consideration given to aerodynamic effects. Additional aerodynamic damping and influence matrices need to be derived. The equations of motion (EOM) that govern the motion of the beam are derived from the principle of virtual work.

Element Matrices and System EOM

From the quasi-steady first-order piston theory, the aerodynamic pressure applied on the beam is

$$P_a = -\frac{2q}{\sqrt{M_\infty^2 - 1}}\left(w_{,x} + \frac{M_\infty^2 - 2}{M_\infty^2 - 1}\frac{1}{V}w_{,t}\right) \tag{1}$$

or

$$P_a = -\left(\lambda\frac{EI}{bL^3}w_{,x} + \frac{g_a EI}{b\omega_0 L^4}w_{,t}\right) \tag{2}$$

where $q = \rho_a V^2/2$ is the dynamic pressure; V is the airflow speed; ρ_a is the air density; M_∞ is the Mach number; and E, I, b, h, and L are property parameters of the beam. The nondimensional dynamic pressure and aerodynamic damping coefficient are given by

$$\lambda = \frac{2qL^3 b}{EI\sqrt{M_\infty^2 - 1}} \tag{3}$$

$$g_a = \frac{\rho_a V\left(M_\infty^2 - 2\right)}{\rho h\omega_0\left(M_\infty^2 - 1\right)^{\frac{3}{2}}} = \sqrt{\lambda C_a} \tag{4}$$

where ρ is the density of the beam, $\omega_0 = (EI/\rho AL^4)^{1/2}$ is the reference frequency, and C_a is aerodynamic damping coefficient ($C_a \approx \mu/M_\infty$ for $M_\infty \gg 1$ and $\mu = \rho_a L/\rho h$ is the mass ratio).

For an Euler–Bernoulli element

$$w = \lfloor N_1 \quad N_2 \quad N_3 \quad N_4 \rfloor (w_1 \quad w_{,x1} \quad w_2 \quad w_{,x2})^T = \lfloor N \rfloor \{d\} \tag{5}$$

thus, we have

$$w_{,x} = \frac{\partial w}{\partial x} = \lfloor N \rfloor_{,x}\{d\}, \qquad w_{,xx} = \frac{\partial^2 w}{\partial x^2} = \lfloor N \rfloor_{,xx}\{d\}$$
$$w_{,t} = \lfloor N \rfloor \{\dot{d}\}, \qquad w_{,tt} = \lfloor N \rfloor \{\ddot{d}\} \tag{6}$$

The strain energy of beam element is

$$U_e = \frac{1}{2}\int_0^{h_e} EI(w_{,xx})^2\,\mathrm{d}x$$

where h_e is element length. With Eqs. (6), the variation of strain energy can be expressed as

$$\delta U_e = \{\delta d\}^T EI \int_0^{h_e} \lfloor N \rfloor_{,xx}^T \lfloor N \rfloor_{,xx}\,\mathrm{d}x\{d\} \tag{7}$$

Similarly, the virtual work done by external forces is

$$\begin{aligned}\delta W_e &= \iint_A \delta w(P_a - \rho h w_{,tt})\,\mathrm{d}A + \delta w F_e \\ &= \{\delta d\}^T \lambda\frac{EI}{L^3}\int_0^{h_e} \lfloor N \rfloor^T \lfloor N \rfloor_{,x}\,\mathrm{d}x\{d\} \\ &\quad - \{\delta d\}^T \frac{g_a}{\omega_0}\frac{EI}{L^4}\int_0^{h_e} \lfloor N \rfloor^T \lfloor N \rfloor\,\mathrm{d}x\{\dot{d}\} \\ &\quad - \{\delta d\}^T \frac{1}{\omega_0}\frac{EI}{\rho AL^4}\rho hb\int_0^{h_e} \lfloor N \rfloor^T \lfloor N \rfloor\,\mathrm{d}x\{\ddot{d}\} \\ &\quad + \{\delta d\}^T \lfloor N \rfloor^T \{F_e\}\end{aligned} \tag{8}$$

With the principle of virtual work $\delta U_e = \delta W_e$,

$$\begin{aligned}&\{\delta d\}^T \frac{1}{\omega_0^2}\frac{EI}{L^4}\int_0^{h_e} \lfloor N \rfloor^T \lfloor N \rfloor\,\mathrm{d}x\{\ddot{d}\} \\ &\quad + \{\delta d\}^T \frac{g_a}{\omega_0}\frac{EI}{L^4}\int_0^{h_e} \lfloor N \rfloor^T \lfloor N \rfloor\,\mathrm{d}x\{\dot{d}\} \\ &\quad + \{\delta d\}^T \lambda\frac{EI}{L^3}\int_0^{h_e} \lfloor N \rfloor^T \lfloor N \rfloor_{,x}\,\mathrm{d}x\{d\} \\ &\quad + \{\delta d\}^T EI\int_0^{h_e} \lfloor N \rfloor_{,xx}^T \lfloor N \rfloor_{,xx}\,\mathrm{d}x\{d\} \\ &\quad = \{\delta d\}^T \lfloor N \rfloor^T \{F_e\}\end{aligned} \tag{9}$$

Thus, the element EOM is

$$\left(1/\omega_0^2\right)[m]\{\ddot{d}\} + (g_a/\omega_0)[g]\{\dot{d}\} + (\lambda[a_a] + [K_e])\{d\} = \{Q_e\} \tag{10}$$

where the element matrices are

$$[m] = [g] = \frac{EI}{L^4}\int_0^{h_e} \lfloor N \rfloor^T \lfloor N \rfloor \, dx$$

$$[a_a] = \frac{EI}{L^3}\int_0^{h_e} \lfloor N \rfloor^T \lfloor N \rfloor_{,x} \, dx$$

$$[K_e] = EI\int_0^{h_e} \lfloor N \rfloor_{,xx}^T \lfloor N \rfloor_{,xx} \, dx$$

$$\{Q_e\} = \lfloor N \rfloor^T \{F_e\}$$

After assembly, the system EOM becomes

$$\left(1/\omega_0^2\right)[M]\{\ddot{W}\} + (g_a/\omega_0)[G]\{\dot{W}\} + (\lambda[A_a] + [K])\{W\} = \{Q\} \tag{11}$$

Solution Procedures

While using frequency-domain analysis to determine the critical dynamic pressure for the traditional self-excited panel flutter problem, the homogenous form of Eq. (11) is used:

$$\left(1/\omega_0^2\right)[M]\{\ddot{W}\} + (g_a/\omega_0)[G]\{\dot{W}\} + (\lambda[A_a] + [K])\{W\} = \{Q\} \tag{12}$$

The flutter boundary can be easily turned into an eigenvalue problem by assuming the response as

$$\{W\} = \{\Phi\}e^{\Omega t} \tag{13}$$

where Ω is generally a complex eigenvalue, $\Omega = \alpha + i\omega$, and α and ω are the panel damping rate and frequency, respectively. By substitution of Eq. (13), Eq. (12) leads to a nondimensional eigenvalue problem of the form

$$\kappa[M]\{\Phi\} = (\lambda[A_a] + [K])\{\Phi\} \tag{14}$$

where the nondimensional eigenvalue is

$$\kappa = -(\Omega/\omega_0)^2 - g_a(\Omega/w_0) \tag{15}$$

This is because that the mass matrix $[M]$ equals the aerodynamic damping matrix $[G]$ as shown in Eq. (10). While there is no airflow, $\lambda = g_a = 0$. The eigenvalues κ are real and positive, corresponding to the square of natural frequencies of free vibration of traditional panel systems (model I, IV, or V). As λ is increased in value monotonically from zero, the symmetric, real stiffness matrix $[K]$ is then perturbed by the skewed aerodynamic influence matrix $[A_a]$ so that two of the eigenvalues approach each other until they coalesce to the value κ_{cr} at $\lambda = \lambda_{cr}$.

The aforementioned impact problem is not applicable to frequency-domain analysis due to the difficulty of describing the boundary condition at the free end (or the impact force). Therefore, simulation of beam time response under airflow and impact force will hopefully unveil the flutter characteristic of the cantilever beam. The equivalent spring has a stiffness of $k_s = E_s A_s / L_s$, where E_s, A_s, and L_s are the Young's modulus, cross-sectional area, and length of the stopper, respectively. Among those popular time integration schemes, the Newmark-β method was adopted here for its stability. The initial conditions used are the first bending mode normalized with $W_{max}/h = 0.1$ and zero initial velocity. Time step length Δt was chosen on the basis of a bisection strategy: The applied time step size is the one giving slightly different critical dynamic pressure compared to the λ_{cr} attained by its double. The ratio W_{max}/h was checked at each time step for judgement of the flutter boundary. The upper limit of W_{max}/h is 4.0, that is, simulation will be ceased as W_{max}/h equals or is greater than 4.0. The impact force is

$$F_e = \begin{cases} 0 & W_e > -\text{gap} \\ -k_s(|W_e| - \text{gap}) & W_e \leq -\text{gap} \end{cases} \tag{16}$$

where W_e is the transverse deflection at the free end of the beam and gap is the size of the gap indicated in Fig. 2.

Results and Discussions

To validate the finite element code the results are compared with available analytical analysis results. However, it is found that for the five members in Fig. 3 no analytical flutter boundaries are presented in the literature. The alternative method adopted here is to check the flutter boundaries of a clamped–clamped beam and both ends of a simply supported beam with the corresponding analytical results.[6] Figure 4 shows that for these two types of supporting conditions (traditional flutter analysis), finite element analysis agrees well with analytical analysis.

Then, the flutter behavior of a steel beam with dimension $L = 1$ in. (0.0254 m), $b = 0.1$ in. (0.00254 m) and $h = 0.006$ in. (1.524×10^{-4} m) was investigated. The beam was discretized with 10 elements. To simulate the tiny gap between the beam free end and stopper top, a gap size of gap$/h = 0.0001$ was employed. Computation was carried out for several distributed stiffness values within the range $k_s = 0 \sim 1.2 \times 10^6$ lbf/in. (2.1×10^8 N/m), with the upper limit corresponding to the steel beam vs steel stopper case. An aerodynamic damping of $C_a = 0.02$ was assumed and used in the analysis.

Figure 5 is the critical dynamic pressure vs spring stiffness curve of the equivalent spring model II. It shows the existence of an

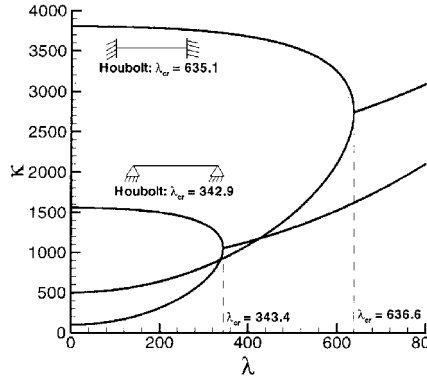

Fig. 4 Critical dynamic pressures: analytical method vs finite element analysis.

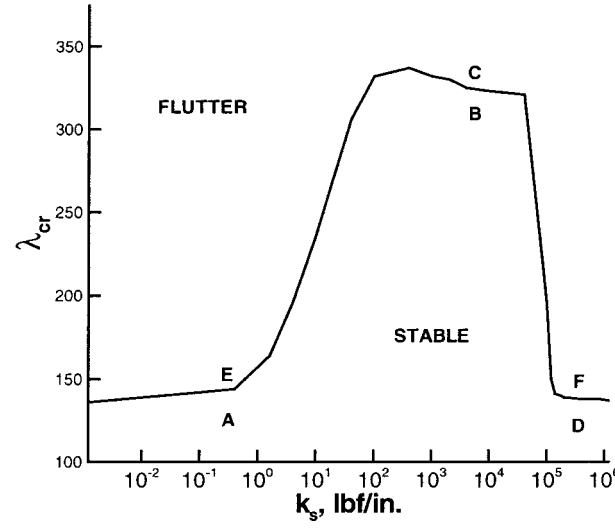

Fig. 5 Flutter boundary of clamped-spring stopper beam.

intermediate stiffness range, roughly, from 40 lbf/in. (7005 N/m) to 40,000 lbf/in. (7.0×10^6 N/m), within which the critical dynamic pressures are over 300. The right and left sides adjacent to this range comprise a low flutter boundary area having nearly the same critical dynamic pressure level as that of the cantilever beam (Fig. 6). The time response and force history of representative points A($k_s = 0.4$, $\lambda = 140$), B($k_s = 2000$, $\lambda = 300$), C($k_s = 2000$, $\lambda = 323$), D($k_s = 200{,}000$, $\lambda = 138$), E($k_s = 0.4$, $\lambda = 160$), and F($k_s = 200{,}000, \lambda = 150$) are shown in Figs. 7–11, respectively. Stable time response has a decaying or limit-cycle oscillation response history (Figs. 7a, 8a, and 10a). Conversely, unstable vibration (flutter) is featured as either the gradual divergence (Fig. 9a) or abrupt increase of $W_{\max}/h$ until the upper limit is reached (Fig. 11).

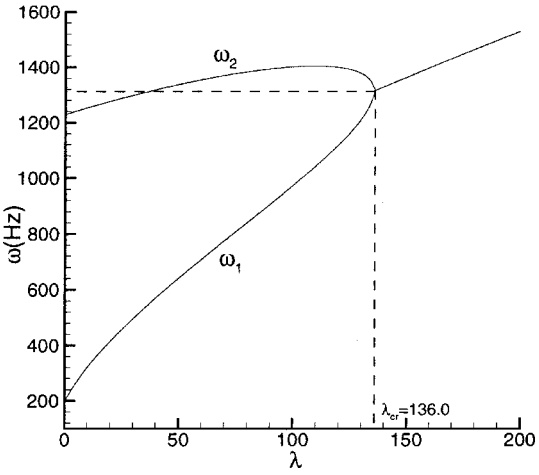

Fig. 6 Cantilever beam critical dynamic pressure.

Point A is below the flutter boundary for the low spring stiffness area. Therefore, as shown in Fig. 7a, the time response is stable. The spring is soft enough that the stopper has little effect on the vibrating beam. Thus, the critical dynamic pressure is very near that of the cantilever beam. This can also be verified by the force shape (Fig. 7d) of one whole impact. The dominating frequency standing out in Fig. 7b is obviously close to the coalescence frequency of the cantilever beam, as can be identified approximately from Fig. 6. While the stiffness increased to the intermediate stiffness area, the rebounce phenomenon denoted by the force shapes in both Figs. 8d and 9d complicated the impact process. Both the stable motion (point B) and unstable motion (point C) are dominated by several modes, instead of the coalescence frequency, as shown in Figs. 8b and 9b. However, it is found that the stiffer the spring stopper is, the smaller the rebounce. Point D is very close to the flutter boundary of $k_s = 200{,}000$, which is $\lambda_{cr} = 139$. Comparing the response power spectrum density (PSD) shown in Figs. 10b and 7b, they have very similar dominating frequencies and shapes. Thus, the critical dynamic pressure of point D should be close to that of the low spring stiffness case. The beat phenomenon observed from Figs. 10a and 10b implies that the lowest two modes are about to coalesce.

Figure 3 listed a family of left end clamped beams with ascending stopper stiffness. Among these five types of beams, the flutter boundaries of cantilever beam (model I), connected spring stopper beam (model IV), and right end simply supported beam (model V) can be determined by frequency-domain analysis. The results are shown in Figs. 6, 12, and 13, respectively.

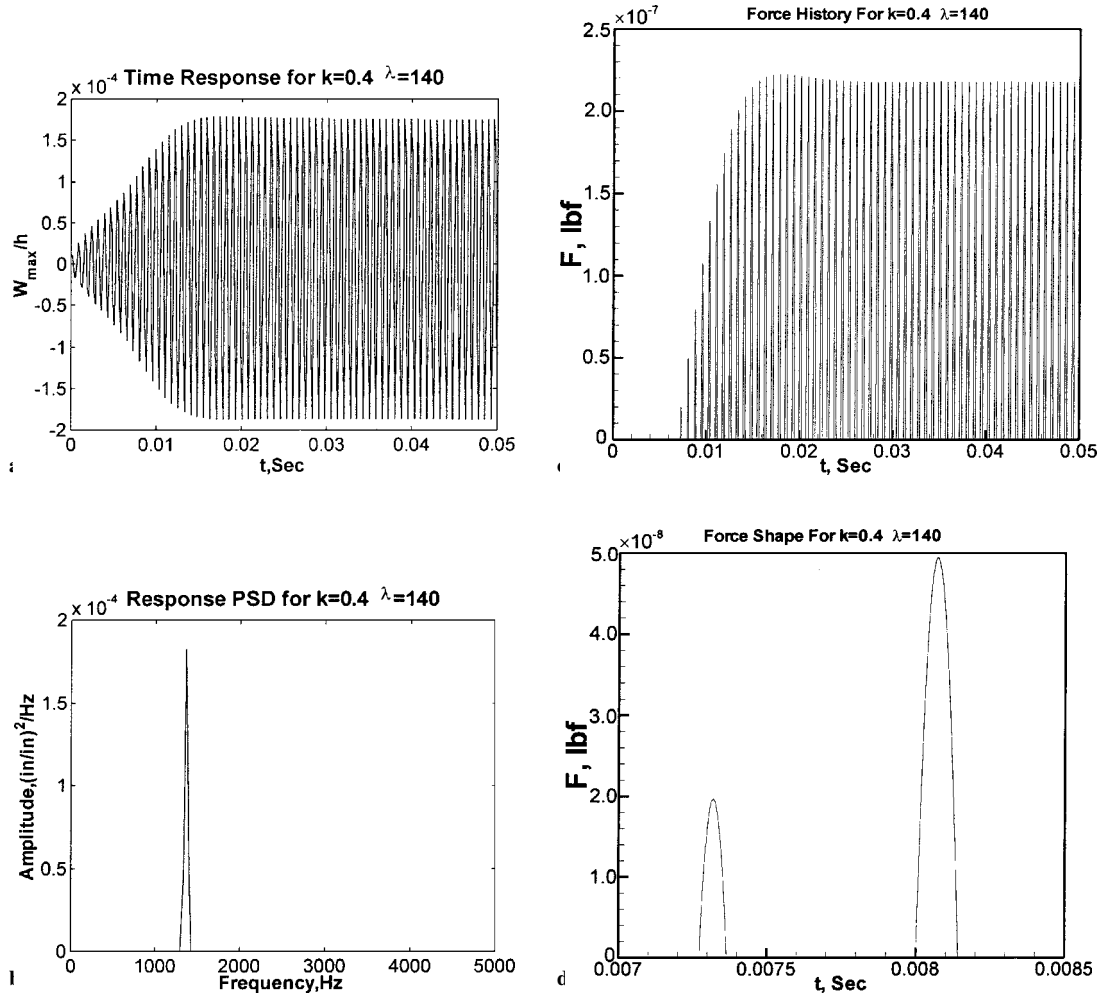

Fig. 7 Response and force characteristics of point A ($k = 0.4$ and $\lambda = 140$).

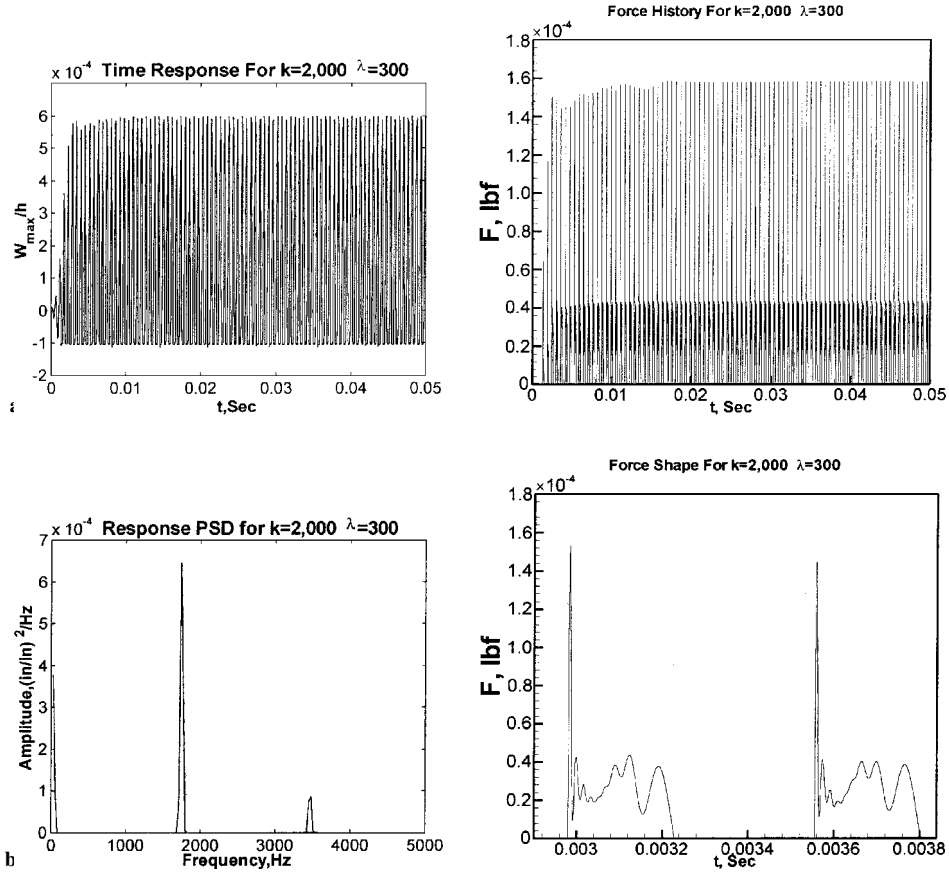

Fig. 8 Response and force characteristics of point B (k = 2000 and λ = 300).

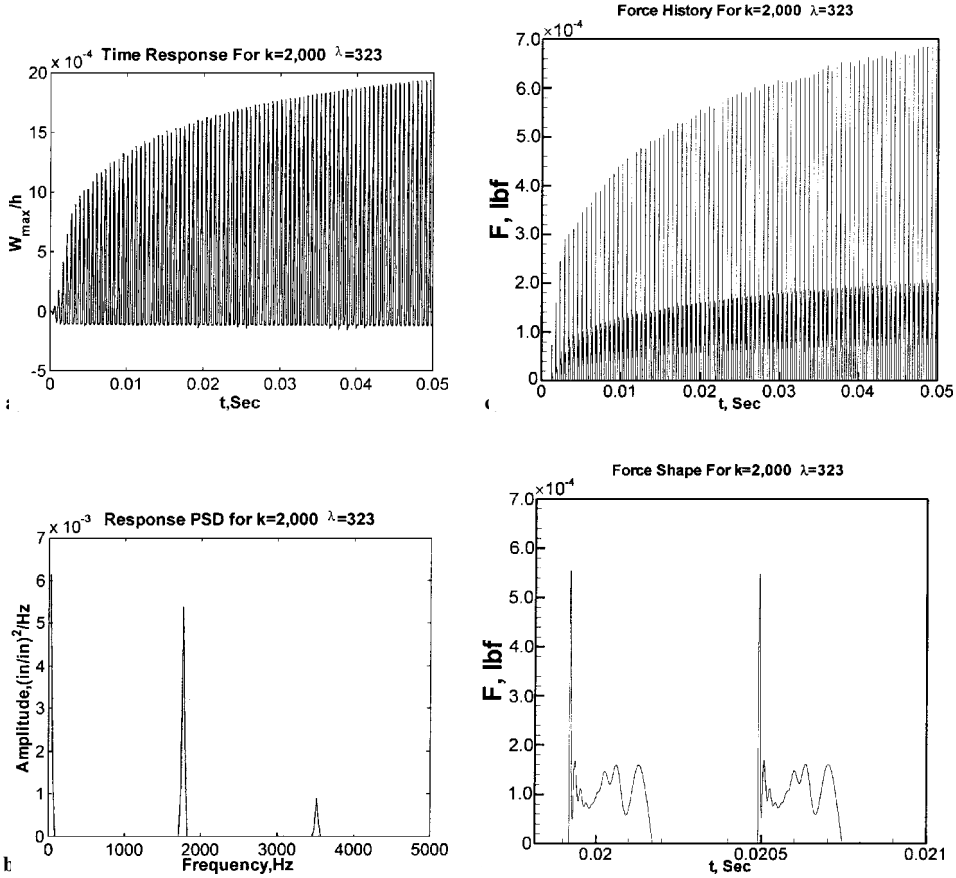

Fig. 9 Response and force characteristics of point C (k = 2000 and λ = 323).

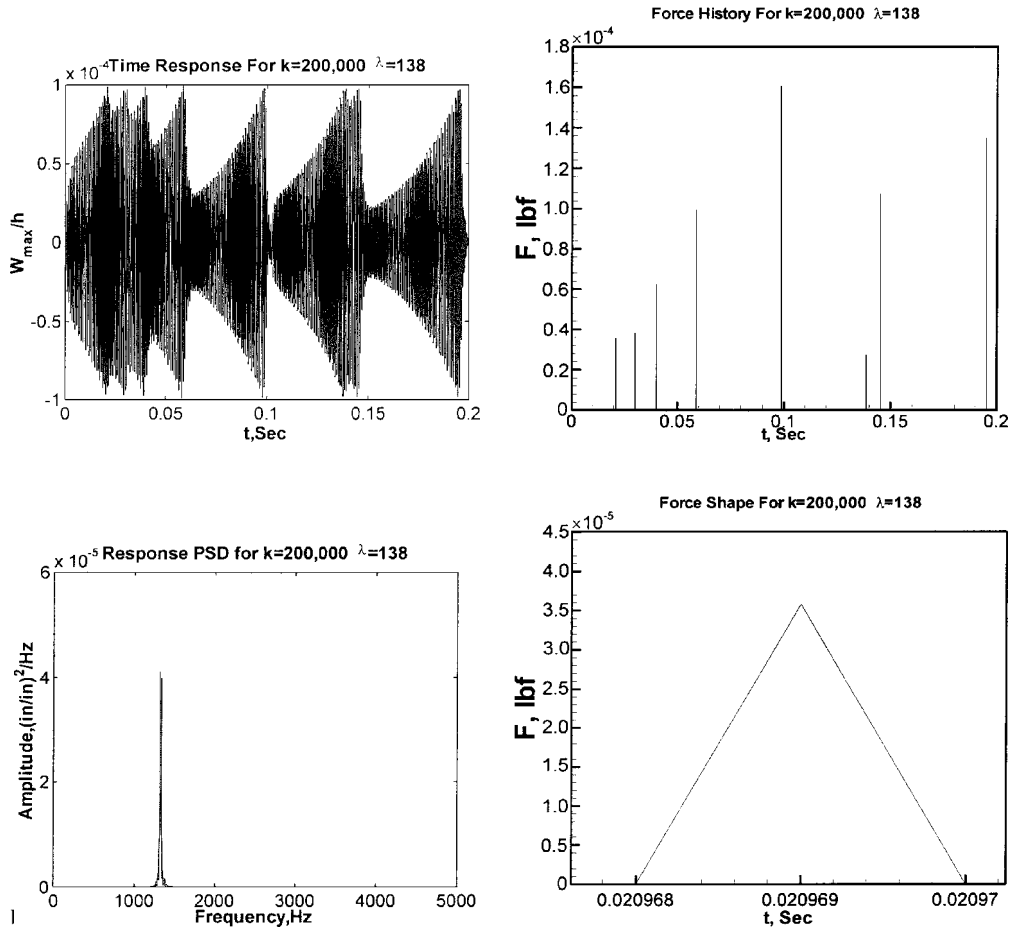

Fig. 10 Response and force characteristics of point D (k = 200,000 and λ = 138).

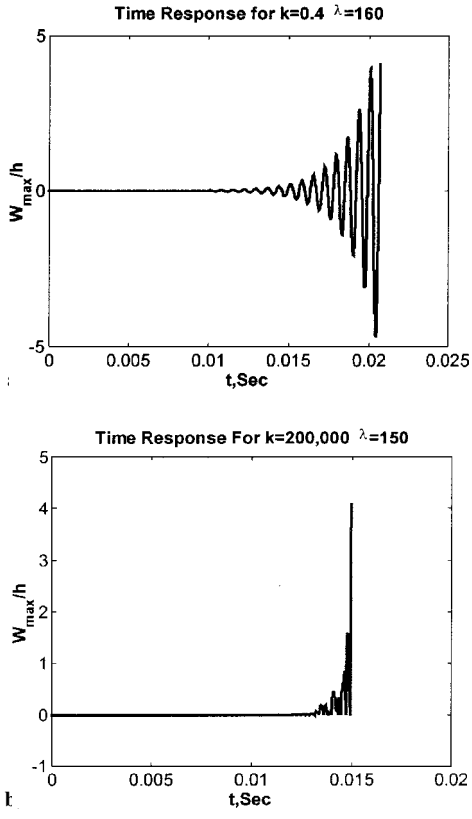

Fig. 11 Time response for a) point E and b) point F.

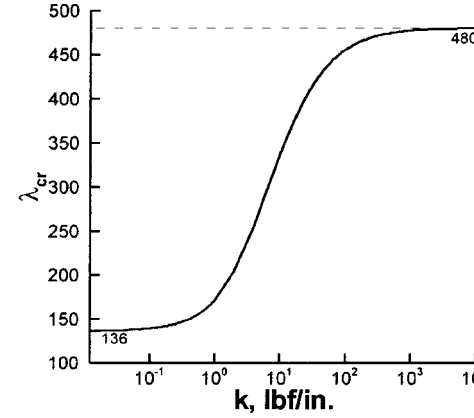

Fig. 12 Flutter boundary of clamped-connected spring beam.

The other two models, spring stopper beam and bar stopper beam, are inapplicable to frequency-domain analysis. The bar stopper beam model is more like the seal of the X-33 TPS panel. The analysis of this model will help with understanding the right-hand side of the curve in Fig. 5. Time-domain analysis was also executed. The 0.25 in. (0.00635 m) long bar stopper has a section area of 0.1×0.1 in.^{2} (6.451×10^{-6} m^2) and is modeled with five bar elements without damping (structural damping will effect the critical dynamic pressure slightly). An understanding of stopper material properties is necessary. Similarly, the Newmark-β method was used as a time integration scheme. Results from analyses of three types of stopper material are listed in Table 1 to show the

Table 1 Critical dynamic pressure of bar stopper beam with stopper modeled as bar elements

Property	Stopper Material		
	Boron	Aluminum	Steel
Density, lb/in.^{3}	0.083	0.098	0.283
Young's modulus E_s, msi	0.0638	8.99	30.2
Equivalent spring stiffness $k_s = E_s A_s / L_s$, lbf/in.	2.55×10^4	3.596×10^5	1.2×10^6
Critical dynamic pressure λ_{cr}	322	140	137

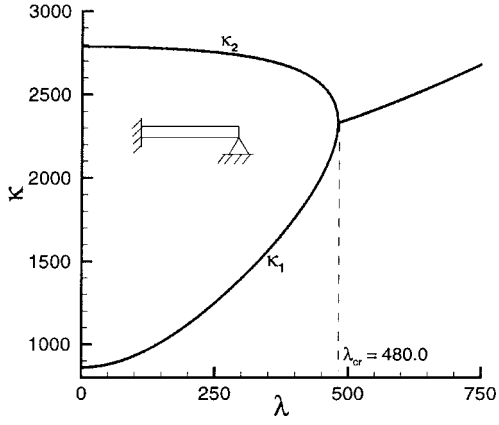

Fig. 13 Critical dynamic pressure of clamped, simply supported beam.

trend of flutter boundary variation. Obviously, the drop of critical dynamic pressure as the stiffness increased to very stiff is confirmed.

Now that the flutter boundaries of all five member beams have been studied, the laws governing them can be addressed. The cantilever beam with $\lambda_{cr} = 136$ comprises both the lower and upper limit cases of the clamped-spring stopper beam. The clamped simply supported beam with $\lambda_{cr} = 480$ is the upper limit case of the connected spring stopper beam. This can be observed from the right-hand end of the curve in Fig. 12. Both the spring stopper beam and connected spring stopper beam exert constraints on the free end of the cantilever beam. Thus, they will enhance the flutter boundary due to stiffening of the whole dynamic system. This is verified by the appearance of similar looking ascending stages appearing in both Figs. 5 and 12. However, the constraint from the spring stopper is unidirectional, and so the spring stopper beam is weaker than the connected spring stopper beam, which applies a bidirectional constraint to the beam. The descending of flutter boundary is then reasonable. Analysis of the bar stopper beam proved this.

Conclusions

In summary, the flutter boundary curve shown in Fig. 5 exposed the character of the original impact problem. The time-domain analysis procedure proved to be valid for flutter analysis of systems with impact boundary conditions. However, it seems that the current work was only the prelude of a systematic work because the practical problem has inevitable effects from temperature, structural damping, etc. Although the model is expanded to a three-dimensional plate and composite materials are considered, predictably, the flow direction effect requires attention.

Acknowledgment

The first and second authors would like to acknowledge the support of Grant NAG-1-2150, NASA Langley Research Center, Hampton, Virginia.

References

[1]Dowell, E. H., "Panel Flutter: Review of the Aeroelastic Stability of Plates and Shells," *AIAA Journal*, Vol. 8, No. 3, 1970, pp. 385–399.

[2]Mei, C., Abdel-Motagalay, K., and Chen, R., "Review of Nonlinear Panel Flutter at Supersonic and Hypersonic Speeds," *Applied Mechanics Reviews*, Vol. 52, No. 10, 1999, pp. 321–332.

[3]Zhou, R. C., Xue, D. Y., and Mei, C., "Finite Element Time Domain–Modal Formulation for Nonlinear Flutter of Composite Panels," *AIAA Journal*, Vol. 32, No. 10, 1994, pp. 2044–2052.

[4]Blosser, M. L., "Development of Metallic Thermal Protection Systems for the Reusable Launch Vehicle," NASA TM 110296, Oct. 1996.

[5]Toulemonde, C., "Periodic Behavior of Impact Oscillators: Single Degree of Freedom and Multiple Degree of Freedom Systems, Experiment," *Proceedings of EUROMECH—2nd European Nonlinear Oscillation Conference*, European Conf. Publications, Cambridge, UK, 1996, pp. 471–474.

[6]Houbolt, J. C., "A Study of Several Aerothermoelastic Problems of Aircraft Structures in High-Speed Flight," Ph. D. Dissertation, Institut für Flugzeugstatik und Leichtbau, Swiss Federal Inst. of Technology, Zurich, 1958.